Size Influences the Effect of Hydrophobic Nanoparticles on Lung Surfactant Model Systems

Mridula V. Dwivedi,[†‡] Rakesh Kumar Harishchandra,[†] Olga Koshkina,[§‖] Michael Maskos,[¶‖] and Hans-Joachim Galla[†*]

[†]Institute of Biochemistry, Westfälische Wilhelms Universität Münster, Germany; [‡]NRW International Graduate School of Chemistry, University of Muenster, Muenster, Germany; [§]BAM Federal Institute for Materials Research and Testing, Berlin, Germany; [¶]Institute of Physical Chemistry, Johannes Gutenberg University, Mainz, Germany; and [‖]Institut für Mikrotechnik Mainz (IMM), Mainz, Germany

ABSTRACT The alveolar lung surfactant (LS) is a complex lipid protein mixture that forms an interfacial monolayer reducing the surface tension to near zero values and thus preventing the lungs from collapse. Due to the expanding field of nanotechnology and the corresponding unavoidable exposure of human beings from the air, it is crucial to study the potential effects of nanoparticles (NPs) on the structural organization of the lung surfactant system. In the present study, we investigated both, the domain structure in pure DPPC monolayers as well as in lung surfactant model systems. In the pure lipid system we found that two different sized hydrophobic polymeric nanoparticles with diameter of ~12 nm and ~136 nm have contrasting effect on the functional and structural behavior. The small nanoparticles inserted into fluid domains at the LE-LC phase transition are not visibly disturbing the phase transition but disrupting the domain morphology of the LE phase. The large nanoparticles led to an expanded isotherm and to a significant decrease in the line tension and thus to a drastic disruption of the domain structures at a much lower number of nanoparticles with respect to the lipid. The surface activity of the model LS films again showed drastic variations due to presence of different sized NPs illustrated by the film balance isotherms and the atomic force microscopy. AFM revealed laterally profuse multilayer protrusion formation on compression but only in the presence of 136 nm sized nanoparticles. Moreover we investigated the vesicle insertion process into a preformed monolayer. A severe inhibition was observed only in the presence of ~136 nm NPs compared to minor effects in the presence of ~12 nm NPs. Our study clearly shows that the size of the nanoparticles made of the same material determines the interaction with biological membranes.

INTRODUCTION

Lung surfactant (LS) is a complex lipid-protein film spanning the air-water interface of the alveoli in the lungs. Its primary function is to reduce the surface tension at the air-water interface, which thus is most essential for the normal breathing process. During the process of inhalation, the reduction in surface tension renders the process effortless and during exhalation, this property prevents the lungs from collapse. In view of the essential functional behavior of the lung surfactant, it is known to reduce the surface tension to near zero values during compression and respread instantaneously without breaking during subsequent expansion (1–3). The mammalian lung surfactant consists mainly of ~85–90% phospholipids and 8–10% of fatty acids, cholesterols, and surfactant-specific proteins (4–6). The dominantly present phospholipids are zwitterionic saturated phosphatidylcholines (PC) (40–50%) primarily responsible for decreasing the surface tension to near zero values (7). However, it has poor respreading properties and rigidifies the surfactant film. To enhance the respreading properties, the second most abundant lipids present are the negatively charged phosphatidylglycerols (PG) and unsaturated phospholipids that fluidize the lung surfactant film. Along with these, surfactant-specific proteins also play a crucial role in the normal functioning of the surfactant film. The surfactant-specific proteins SP-B and SP-C are mainly involved in enhancing the surface activity of the surfactant film during compression and expansion (5,8). Whereas SP-A and SP-D are related to the immunological and host defense mechanism (9). Over the years, a good amount of literature has cleared our knowledge about action of the lung surfactant film. On compression, the fluid components of the lipid-protein monolayer squeeze out to form three-dimensional (3D) multilayer stacks or protrusion structures, which acts as a surfactant reservoir. On expansion, these multilayer stacks are reincorporated into the monolayer and assist the respreading of the film to form a stable lung surfactant film. The presence of these structures in vivo has been evidenced by atomic force microscopy (AFM) and electron microscopy (EM) studies. These multilayer stacks are formed and held together by the aid of SP-B and SP-C and hence the lipid and protein components of the surfactant film interact and harmonize with each other during the breathing cycle (10–13). The surfactant-specific proteins SP-B and SP-C also play an important role in the recycling and replenishment of the lipid material by the vesicle insertion process (14–16).

Although advances in nanotechnology has brought to us novel methods in medical diagnostics and targeted drug

Submitted May 17, 2013, and accepted for publication October 10, 2013.

*Correspondence: gallah@uni-muenster.de

Rakesh Kumar Harishchandra's present address is Department of Chemistry and Biochemistry, Worcester Polytechnic Institute (WPI), 60 Prescott Street, Worcester, MA 01605.

Editor: Klaus Gawrisch.

0006-3495/14/01/0289/10 $2.00

http://dx.doi.org/10.1016/j.bpj.2013.10.036

delivery, it has also made us prone to exposure of nanoparticles (NPs) through inhalation from the atmosphere. It is hence of utmost importance to study the effect of the intentional or unintentional exposure of nanosized particles to the lung surfactant. The important parameters to be investigated in these nanoparticle interaction studies are—disturbance of the structural and functional behavior of the LS film, interaction with the individual components of the LS film, retention/penetration of the NPs in the film, and interaction with epithelial cells and alveolar macrophages. Recently, numerous amounts of research have been dedicated to monitor the toxicological influence of different kinds of NPs on the lungs and the further fate of the NPs (17–19). A few reports have focused on the lung surfactant dysfunction caused by the inhalation and penetration of NPs through the lung surfactant film. In most cases, the lung surfactant dysfunction has been caused in a dose- and time-dependent manner by the frequently used metallic NPs, which indeed form a major part of the particulate matter in the atmosphere and are also employed in medical diagnostics (20–23). However, seldom have the dosages been physiologically relevant. It has also now become clear that the toxicological effect of NPs are more or less dependent upon the surface properties, shape, size, solubility, and surface charge of the NPs (24). It has been previously shown that 20 nm AmorSil20 polymeric hydrophobic NPs tend to inhibit the lung surfactant function at high concentrations and a detailed study employing various applications of AFM and EM showed that these hydrophobic NPs are retained into the surfactant film even after repetitive compression expansion cycles (22,25). This behavior of a few NPs to retain into the surfactant film could be exploited by the drug delivery applications for long-term release of the drugs into the system before the NPs are cleared out. Hence, these NPs are required to cause minimal disturbance to the lung surfactant function. In this report, we have studied the effect of size of NPs on the biophysical behavior of model LS films and proved that the size of the NPs is an important factor responsible for causing severe damage to the lung surfactant structure.

In view of the highly complex and dynamic nature of the natural lung surfactant film, it is technically challenging to extract any valuable information from such a system and hence a well-characterized and highly reproducible model system has been developed that closely mimics the natural lung surfactant. It consists mainly of the zwitterionic 1,2-dipalmitoyl-*sn*-glycero-3-phosphocholine (DPPC), negatively charged 1,2-dipalmitoyl-*sn*-glycero-3-phosphoglycerol (DPPG) and surfactant-specific protein SP-C (26–28). In this study, we have investigated the influence of size of hydrophobic polymeric NPs on the lung surfactant model system. We have studied the variation in the surface activity of the lung surfactant model system in the presence of small NPs (diameter = 12.4 ± 2.6 nm, determined by transmission electron microscopy (TEM), particles deposited from chloroform) and large NPs (diameter = 136 ± 27.0 nm, TEM, particles deposited from chloroform) with the same surface characteristics as the previously studied NPs (AmorSil20) with a diameter ~20 nm consisting of inert Si-CH3 groups making it essentially hydrophobic in nature. The evidently contrasting surface activity behavior of the lung surfactant model system in the presence of different sized NPs has been further explored using the AFM technique. The factors that are focused upon in this study are—variation in the surface activity of the LS model system and hence inhibition of surfactant function, the effect of size variance on the line tension and domain morphology, the effect of size on the 3D protrusion structures, localization of the different sized NPs around the protrusion structures, and analysis of the multilayer steps of the protrusion structures. Furthermore, the size-dependent effect of hydrophobic NPs on the vesicle insertion process is studied by vesicle insertion kinetic studies.

MATERIALS AND METHODS

Materials

DPPC and DPPG were purchased from Avanti Polar Lipids (Alabaster, AL). SP-C was isolated from porcine bronchoalveolar lavage fluid by the butanol extraction method (29,30). 2-(4, 4-Difluoro-5-methyl-4-bora-3a, 4a-diazas-indacene-3-dodecanoyl)-1-hexadecanoyl-*sn*-glycero-3-phosphocholine (*β*-BODIPY 500/510 C_{12}-HPC, BODIPY-PC) was purchased from Molecular Probes (Eugene, OR). Chloroform and methanol were high pressure liquid chromatography grade and obtained from Sigma-Aldrich (Steinheim, Germany) and Merck (Darmstadt, Germany), respectively. *N*-(2-Hydroxyethyl) piperazine-*N*′-(2-ethanesulfonic acid) sodium salt (Na-HEPES), and calcium chloride ($CaCl_2$) were purchased from Sigma-Aldrich. Water was purified and deionized by a multicartridge system (Sartorius, Goettingen, Germany) and had a resistivity >18 MΩm at 25°C. Lipids were dissolved in chloroform/methanol solution (1:1, v/v). All chemicals were used as received: trimethoxymethylsilane, diethoxydimethylsilane, (p-chloromethyl)phenyltrimethoxysilane, (ABCR, Germany), dodecylbenzenesulfonic acid, chloroform (Sigma-Aldrich).

Sample preparation

Poly(organosiloxane) NPs were synthesized by condensation of di- and trialkoxysilanes as described previously (31–33). Briefly, the synthesis of 12 nm core-shell NPs (R = 6.2 ± 1.3 nm (TEM)) was carried out under alkaline conditions using benzethonium chloride as surfactant at a fleet ratio of 0.3. The core was fluorescently labeled by addition of rhodamine B-(p-trimethoxysilyl)benzylester to the monomer mixture. 136 nm NPs (R = 68 ± 13.5 nm (TEM)) were prepared with dodecylbenzenesulfonic acid as surfactant (fleet ratio 0.001) by sequential condensation of polydimethylsiloxane-core and two shells; the inner shell was labeled by rhodamine B during polycondensation.

The characterization of particle size in aqueous solution was carried out by multiangle dynamic light scattering (DLS) using an ALV/CGS-3 Compact Goniometer System, with HeNe Laser ($\lambda_0 = 633$ nm). All samples were filtered (Millex-LCR filter, 0.45 μm pore size, Millipore) before measurement. For determination of hydrodynamic radii, the autocorrelation data were evaluated by applying a biexponential fit, $\mu 2$ values were derived from a cumulant fit at 90° (34). DLS measurements showed a hydrodynamic radius R_h of 7.9 nm ($\mu 2 = 0.11$) for 12 nm particles and R_h of 70.9 nm ($\mu 2 = 0.05$) for 136 nm particles in aqueous dispersion.

After polycondensation and characterization by DLS the free silanol groups on the nanoparticle's surface were endcapped with trimethylethoxysilane. The particles were washed or dialyzed in methanol to remove the surfactant. By this procedure the surface properties of the NPs were changed to hydrophobic and the particles were redispersed in chloroform and visualized by TEM (33). The hydrodynamic radii of the hydrophobic particles were determined by DLS in tetrahydrofuran. The resulting values are $R_h = 110$ nm (μ_2 (90°) = 0.06) for the big particles and $R_h = 9.1$ nm (μ_2 (90°) = 0.07) for the small particles.

The NPs were dissolved in chloroform to obtain 3.784×10^{12} NPs/mL (5.98 mg/mL) of 136 nm NPs stock solution and 1.430×10^{16} NPs/mL (17.13 mg/mL) of 12 nm NPs stock solution. The NPs were mixed in lipid solutions (1 mg/mL) in concentrations of 1, 10, 20, 50, 100, and 1000 μg/mL for both 136 nm and 12 nm NPs to acquire physiological relevance and hence the number of NPs in the case of 136 nm NPs is 10^3 times smaller than that of 12 nm NPs. The lipid-nanoparticle mixture, dissolved in chloroform/methanol (1:1, v/v) solution, was sonicated and injected onto the subphase.

Surface pressure-Area isotherms

All the film balance experiments were performed on an analytical Wilhelmy film balance (Riegler and Kirstein, Mainz, Germany) with an operational area of 144 cm^2. All surface pressure measurements were done on 25 mM HEPES with 3 mM $CaCl_2$ at pH 7.0 as buffered subphase at 20°C. The sample solutions consisting of lipid mixtures and NPs was injected onto the subphase and was left for an equilibration time of 10–15 min for the solvent to evaporate after which the lipid monolayer formed was compressed at the rate of 2.9 cm^2/min using a Teflon barrier.

The monolayer isothermal compressibility of the DPPC film was calculated using

$$\mathbf{C}_s = (-1/A)(dA/d\pi),$$

where $\mathbf{C}_s$ is the compressibility coefficient, A is the molecular area at a given surface pressure, and π is the corresponding surface pressure. The compressibility coefficient is known to indicate the lateral stiffness of the monolayer at a given surface pressure.

Video-enhanced epifluorescence microscopy

Domain structures of DPPC in the presence of NPs were observed by doping the lipid solution with 0.5 mol% BODIPY-PC and visualizing by means of an epifluorescence microscope (Olympus STM5-MJS,Olympus, Hamburg, Germany) equipped with *xy*-stage and connected to a charge-coupled device camera (Hamamatsu, Herrsching, Germany). The images were captured at desired surface pressures by stopping the barrier. All the measurements were done in pure water as the subphase at 20°C.

Langmuir-Blodgett transfer

The lipid mixtures with and without NPs were spread onto the 25 mM HEPES with 3 mM $CaCl_2$ at pH 7.0 subphase in a film balance (Riegler and Kirstein) with an operational area of 39 cm^2 and the monolayer obtained was compressed with a velocity of 1.5 cm^2/min to achieve the desired surface pressure and area per molecule. The lipid film was allowed to stabilize at the attained surface pressure and area per molecule for around 10 min and then an already positioned vertically dipped freshly cleaved mica sheet is drawn upward with the speed of 0.7 mm/min. For the lipid film with 12 nm NPs, this transfer is carried out at around 52.2 mN/m, i.e., at the plateau region where multilayer protrusion structures are observed. For the lipid mixture with 136 nm NPs, the film is transferred at the beginning of the plateau and at the end of the plateau where the surface pressure is around 50.5 mN/m in either case. The area per molecule value is attained by slowly stopping the barrier at the desired position and stabilizing the lipid film for around 10 min before beginning the transfer. All the transfers were done at 20°C.

AFM

The Lipid films transferred onto the mica sheet were scanned using NanoWizard III (JPK Instruments, Berlin, Germany). Silicon nitride tips (Budget Sensors, Sofia, Bulgaria) with a spring constant of 40 N/m and a resonance frequency of 300 ± 100 kHz were used. All the scanning was performed in the intermittent contact mode in air at 20°C. The images were obtained at 512 × 512 pixel resolution and processed using JPK data processing software.

Vesicle insertion kinetic studies

Vesicle preparation

A phospholipid mixture containing DPPC/DPPG in the molar ratio 4:1 were dissolved in a chloroform/methanol (1:1, v/v) solution and dried under a stream of nitrogen at 50°C. Traces of solvent were removed for at least 3 h at 50°C in a vacuum oven. The dried lipid films were then hydrated by adding a buffer containing 25 mM Hepes and 0.1 mM EDTA. The suspension was kept for 30 min at 50°C water bath and vortexed every 10 min. The resulting multilamellar vesicles solution was extruded from a 100 nm pore size polycarbonate membrane to obtain a 100 nm large unilamellar vesicle solution.

Vesicle insertion studies

The insertion experiments were performed using model LS monolayer on 25 mM Hepes and 3 mM $CaCl_2$ at pH 7.0 as buffer subphase at 20°C. The lipid film with and without NPs was spread at the air-water interface on a film balance (Riegler and Kirstein) with an operational area of 39 cm^2 and the monolayer obtained was compressed with a velocity of 1.5 cm^2/min to achieve the desired surface pressure (25 mN/m in this case). The lipid film was stabilized for at least 10 min before injecting the large unilamellar vesicle (LUV) solution into the subphase. The increase in surface pressure is measured with respect to time and the isotherm obtained is used for analyzing the insertion kinetics of the model LS film in the presence of different sized NPs.

RESULTS

Size-dependent effect of NPs on surface activity of DPPC monolayer

The size-dependent effect of hydrophobic NPs on the surface activity of DPPC monolayers was studied using the Langmuir film balance. DPPC forms the major component of the model LS film and hence alteration in its phase behavior consequently causes alteration in the phase behavior of model LS films. The isotherm of a pure DPPC monolayer consists of an initial gaseous phase succeeded by a liquid-expanded phase (LE), a liquid-condensed (LC) phase, and a solid phase. The phase transition from the LE phase to the LC phase is intermediated by the LE-LC phase coexistence region, which is signified by a plateau at a surface pressure of around 5 mN/m. The isotherms illustrating the size-dependent effect of NPs on DPPC monolayer are presented in Fig. 1. In the presence of 12 nm

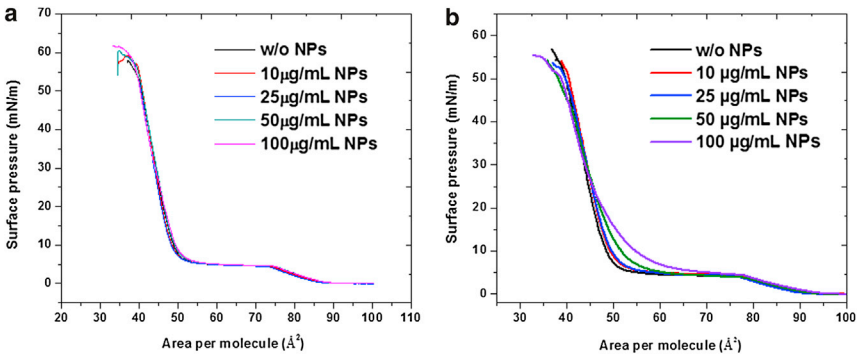

FIGURE 1 Surface pressure-Area per lipid molecule isotherm for (*a*) DPPC + 12 nm NPs and (*b*) DPPC + 136 nm NPs with 25 mM Hepes + 3 mM $CaCl_2$ as the subphase. To see this figure in color, go online.

NPs no change in the isotherm occurred up to the measured concentrations (Fig. 1 *a*). However, in the presence of 136 nm NPs, the isotherm is expanded toward a higher area per molecule values diminishing the LE-LC coexistence region (Fig. 1 *b*).

The compressibility values (C_s) (Table 1) are calculated for the DPPC films in the LC phase at the area per molecule value of 45 $Å^2$. With increasing concentration of the 136 nm NPs the compressibility values increased for the DPPC monolayer.

Size-dependent effect of NPs on line tension and domain morphology of DPPC monolayer

A lipid monolayer forms phase separated domains on compression depending on the surface pressure. The domain morphology can be studied using epifluorescence microscopy by doping the lipid monolayer with BODIPY-PC dye, which is known to preferentially partition into the LE phase. Hence, the LC phase appears as dark domains.

The size-dependent effect of NPs on the domains formed by DPPC films is presented in Fig. 2. Increasing concentrations of 12 nm NPs cause disruption of the domain morphology beginning with formation of outgrowths at the periphery of the LC domains at low concentrations of the NPs (Fig. 2 *a*). The fluorescent NPs are visible at high surface pressure values as bright stretches (shown in *red*) against the compressed lipid monolayer background because of the fluorescent Rhodamine B core of the nanoparticles.

With increasing concentrations of 136 nm NPs the LC domains form branched structures, which at high surface pressure forms a mesh-like network (Fig. 2 *b*). The significant decrease in the line tension between phases responsible for domain morphology is noticeable along with profuse disruption of the domain structures. The effect is considerably strong even at a very low concentration of 1 μg/mL, which amounts to a much lower number of NPs (10^6 lipid molecules per nanoparticle) as compared to that of 12 nm NPs (10^2 lipid molecules per nanoparticle) (Fig. S2 in the Supporting Material).

Hence, the presence of 136 nm NPs significantly alters the phase behavior of DPPC monolayers and decreases phase separation. To further understand the size-dependent effect of NPs on model LS films, a DPPC/DPPG/SP-C (80:20:0.4 mol%) mixture was used.

Size-dependent effect of NPs on surface activity of LS model system

The characteristic surface pressure-area isotherm for a pure DPPC/DPPG/SP-C (80:20:0.4 mol %) lipid mixture shows a continuous increase in the surface pressure upon compression until it reaches the surface pressure value of around 52 mN/m. There it forms a plateau signifying a squeeze out of some of the lipid component of the monolayer, thus preventing an increase in the surface pressure values for around 5–10 $Å^2$ area per molecule region. This is explained by the selective squeeze out of the fluid component of the lipid monolayer forming multilayer stacks held together by surfactant-specific proteins (SP-C in this case).

The size-dependent effect of NPs on the surface properties of the LS model system is illustrated in Fig. 3. The presence of 12 nm NPs in the LS model system monolayer does not cause any significant change in the surface pressure-area isotherm except at a very high concentration where the plateau formation is inhibited (Fig. 3 *a*).

With increasing concentration of 136 nm NPs, however, the plateau region of the LS film isotherms is enhanced unlike for 12 nm NPs (Fig. 3 *b*). At the highest concentration of 136 nm NPs that we measured (i.e., 100 μg/mL), the compressibility of the lipid film at the plateau region is increased immensely to achieve very low area per molecule values on continuous compression. In addition, we observed

TABLE 1 Compressibility values for DPPC film at the area per molecule value of 45.1 $Å^2$ in LC region on 25 mM HEPES + 3 mM $CaCl_2$ buffer subphase in the presence of varying concentrations of 136 nm NPs at 20°C.

	w/o NPs	10 μg/mL NPs	25 μg/mL NPs	50 μg/mL NPs	100 μg/mL NPs
C_s(m/mN)	3.92×10^{-3}	4.0×10^{-3}	4.45×10^{-3}	6.0×10^{-3}	7.08×10^{-3}

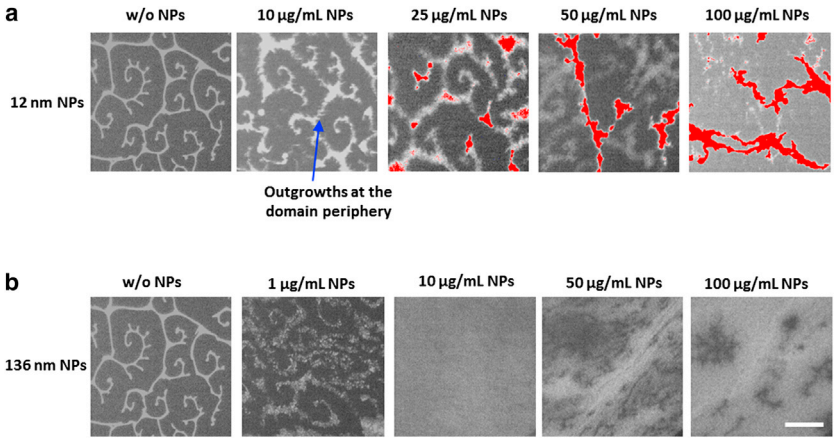

FIGURE 2 Epifluorescence microscopy images for DPPC in the presence of increasing concentration of (*a*) 12 nm NPs and (*b*) 136 nm NPs on water as the subphase at 20°C. The DPPC monolayer is doped with 0.5 mol% BODIPY-PC, which preferentially partitions into the LE phase. The images are taken at 10 mN/m surface pressure. Scale bar is 50 μm. To see this figure in color, go online.

a slight expansion of the isotherm toward higher area per molecule values with increasing nanoparticle concentration. From the repetitive cyclic compression expansion cycles for the model LS system in the presence of 12 nm as well as 136 nm NPs, we observed no variation in the hysteresis effect suggesting that there is no loss of material from the lipid monolayer into the subphase in either case (Fig. S3). This also implies the retention of NPs in the lipid monolayer after three compression and expansion cycles for both 12 nm as well as 136 nm NPs.

Surface activity studies of bare NPs

To study the surface activity of bare NPs, the nanoparticle solutions were spread onto the buffered subphase and compressed to achieve very low area per nanoparticle values as technically feasible. Using film balance, often, molecular arrangements can be contemplated based on the surface activity of the molecules (or particles) of interest. Higher surface activity for a wide range of area per nanoparticle implies a higher level of interaction between the molecules and hence lesser affinity between the NPs and the aqueous subphase. This consequently gives an idea of the hydrophobicity of the nanoparticle and hence the high free energy barrier encountered by the NPs to enter into the subphase.

As shown in Fig. S4 the wide range of area per molecule values for 136 nm NPs reveal the high surface activity of these particles, which can be compressed to very low area per nanoparticle values without collapsing into the subphase. The 12 nm NPs, on the other hand, show comparatively less surface activity properties and display a sudden increase in surface pressure and a sudden collapse on compression. The wider range of surface activity can be explained by the very high free energy barrier encountered by the 136 nm hydrophobic NPs at the aqueous interface to enter into the aqueous subphase. The free energy barrier is also encountered by the 12 nm NPs; however, the free energy barrier experienced by the 136 nm NPs is much larger inhibiting the collapse of the NPs into the subphase.

Size-dependent effect of NPs on multilayer protrusion structures

To study the surface topology of the LS model system at the plateau region in the presence of both 12 and 136 nm NPs the AFM technique was used. The lipid film was transferred at the plateau region of the isotherm from the aqueous surface onto a solid substrate and scanned under AFM. To study the surface topology of the model LS film in the presence of 136 nm NPs at the enhanced plateau region,

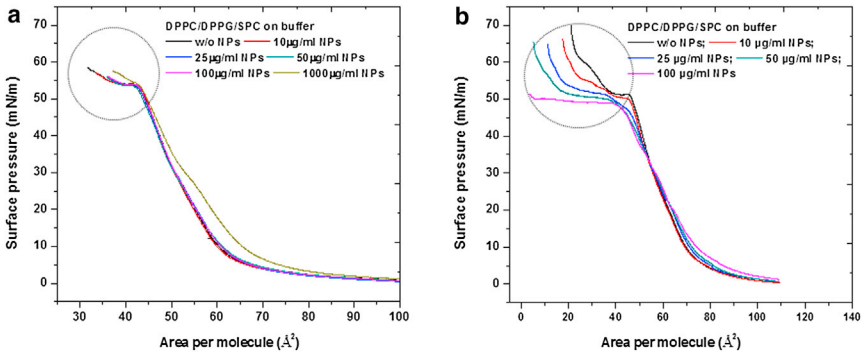

FIGURE 3 (*a*) Pressure-Area isotherm for DPPC/DPPG/SP-C (80:20:0.4 mol%) + 12 nm NPs. (*b*) Pressure-Area isotherm for DPPC/DPPG/SP-C (80:20:0.4 mol%) + 136 nm NPs. All measurements were done on 25 mM Hepes + 3 mM $CaCl_2$ as the subphase at 20°C. To see this figure in color, go online.

the lipid film was transferred at both the initial plateau region and at the end plateau region.

The AFM scan for pure DPPC/DPPG/SP-C (80:20:0.4 mol%) monolayer lipid film at the plateau region shows network structures that are multilayer protrusions as previously observed (22).

Surface topology analysis of LS model system in the presence of 12 nm NPs

The protrusion structures are not affected noticeably by the presence of 12 nm NPs, in the applied concentration (Fig. 4 *b*). They are visibly localized around the protrusion structures (marked by *arrows*). High-resolution scanning confirms the presence of NPs associated with the protrusion structures (see Fig. 5 *a*).

Surface topology analysis of LS model system in the presence of 136 nm NPs

AFM scans for the LS model system in the presence of 136 nm NPs reveal a significant lateral disruption of the network structures (Fig. 4, *c* and *d*). At the initial plateau region, the network structures consisting of multilayer protrusions are intact (Fig. 4 *c*). However, at the end plateau region, the network structures are considerably disrupted forming laterally disordered profuse multilayer protrusions (Fig. 4 *d*). With increasing concentration of NPs the lateral disorder increases significantly as shown in Fig. S6. The highest clusters with a height of around 100 nm (marked by *arrows*) were imaged under high resolution. These images clearly show the presence of 136 nm NPs associated with the protrusion structures (Fig. 5 *b*). The topography images are supplemented by phase images that have higher clarity revealing a cluster of NPs (Fig. 5 *c*). It should be noted that the size measured for these NPs are in aqueous dispersions. However, the 136 nm NPs present on the mica substrate within the LS model system film are dried rendering the size to be around 100 nm because of the elastic properties manifested by the 136 nm NPs.

The 136 nm NPs visible in the phase images are similar to those obtained in TEM micrograph images (Fig. S7). The

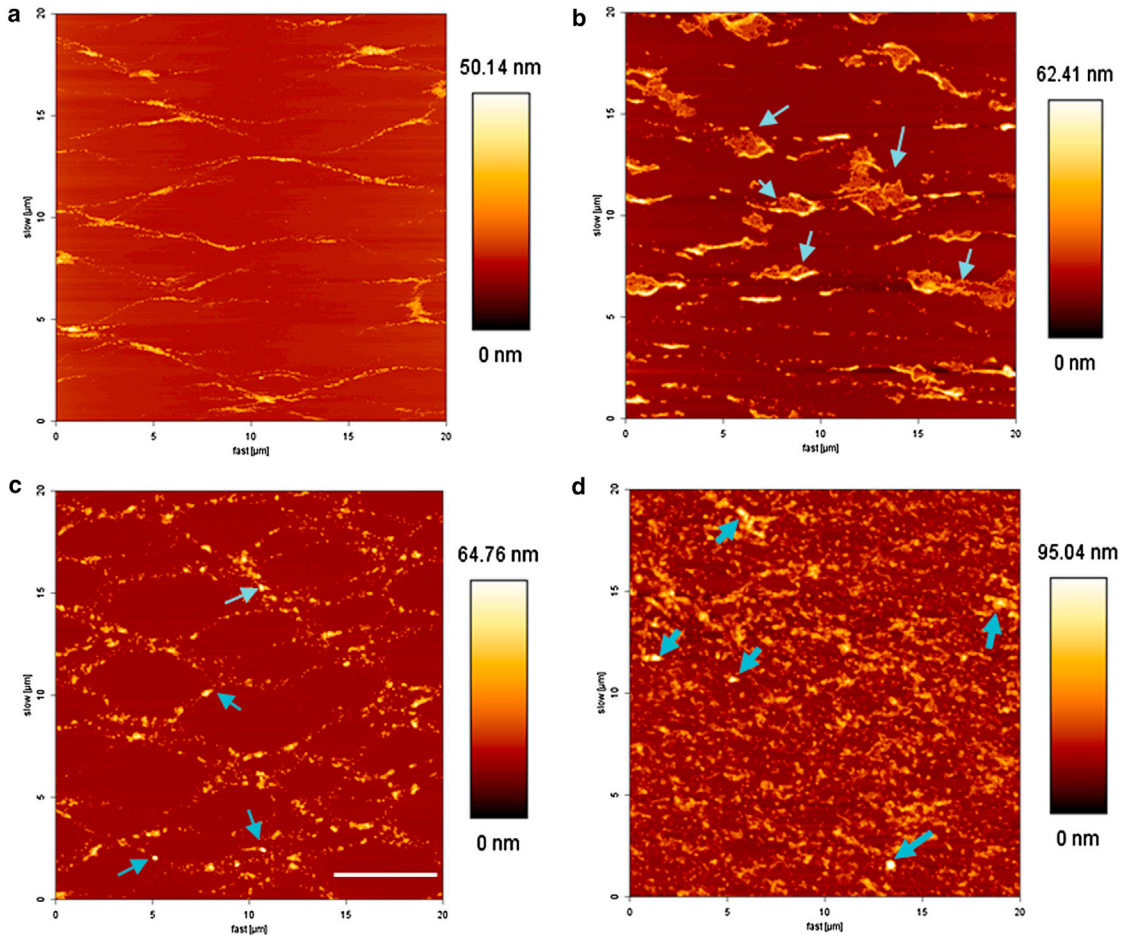

FIGURE 4 AFM topography images of (*a*) pure DPPC/DPPG/SP-C (80:20:0.4 mol%) monolayer lipid film; (*b*) with 100 μg/mL 12 nm NPs at plateau region; (*c*) with 100 μg/mL 136 nm NPs transferred at initial plateau region; (*d*) with 100 μg/mL 136 nm NPs at end plateau region. The film was compressed on 25 mM Hepes + 3 mM $CaCl_2$ as the subphase at 20°C. The clusters of NPs around the protrusion structures are marked by arrows. Scale bar is 5 μm. To see this figure in color, go online.

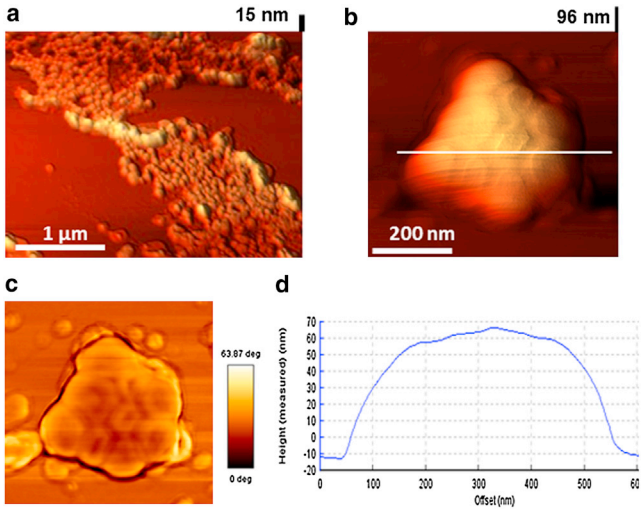

FIGURE 5 High-resolution imaging for DPPC/DPPG/SP-C (80:20:0.4 mol%) monolayer lipid films. (*a*) 3D topography image with 12 nm NPs; (*b*) 3D topography image with 136 nm NPs; (*c*) Phase images showing 136 nm NPs with higher clarity; (*d*) Height profile analysis for 136 nm NPs clusters. To see this figure in color, go online.

136 nm NPs appear to be nonrigid as evidenced by surface deformation during packing (Fig. 5 *c*, Fig. S7 *b*). Hence, the negative phase change at the top of the 136 nm NPs could be explained by the ability of the cantilever to press into the nanoparticle during measurement. The height profile of the nanoparticle cluster shows height up to 100 nm with curved edges corresponding to the shape of the nanoparticle.

As shown by the hysteresis studies, the continuous compression of the LS model system film in the presence of 136 nm NPs does not show any irreversible damage to the model surfactant film due to a loss of any component into the subphase (Fig. S3). This is consistent with the AFM studies, which show the formation of multilayer steps with step heights of 5 nm, i.e., for a bilayer (Fig. 6, marked by *arrows*) around the NPs. Hence, in the presence of 136 nm NPs, the structures formed are indeed multilayer protrusion structures and not collapse structures due to a disruption of the film.

Effect of nanoparticle size on vesicle insertion kinetics of model LS films

The natural LS monolayer is constantly recycled and replenished with new lipid material from the subphase by the vesicle insertion process. This process is essential for maintaining the integrity and functional activity of the lung surfactant monolayer (32). We have tried to mimic this process by inserting DPPC/DPPG (4:1) LUVs into the subphase containing model LS film at the air-water interface. The model LS monolayer is compressed up to 25 mN/m, stabilized for 10 min, and the LUVs are inserted into the subphase. The increase in surface pressure is monitored with time to obtain an isotherm, which gives information about the insertion kinetics of the vesicles into the monolayer.

Fig. 7 illustrates the effect of different sized NPs on the vesicle insertion kinetics of model LS monolayer. The presence of higher numbers of 12 nm NPs does not cause a significant effect on the vesicle insertion process of this model LS film. However, in the presence of a comparatively lower number of 136 nm NPs, the vesicle insertion process is considerably inhibited.

DISCUSSION

Previously, we studied the effect of hydrophobic NPs (AmorSil20) with a diameter of 20 nm and showed that these NPs are localized around the multilayer protrusion structures. The NPs with 20 nm diameter did not cause any significant damage to the lung surfactant surface activity except at a very high concentration of 1000 μg/mL wherein the plateau formation was inhibited. The multilayer protrusion structures consequently were also unaffected by

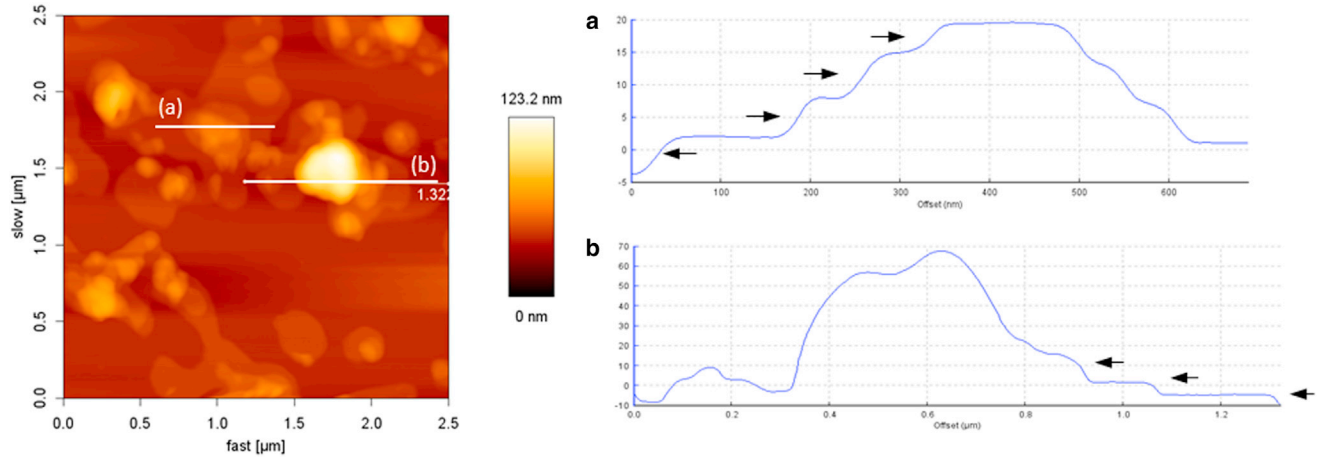

FIGURE 6 AFM images of for DPPC/DPPG/SP-C (80:20:0.4 mol%) monolayer lipid films with 136 nm NPs showing presence of multilayer steps (marked by *arrows*). The AFM image is accompanied by its height profiles to the right. To see this figure in color, go online.

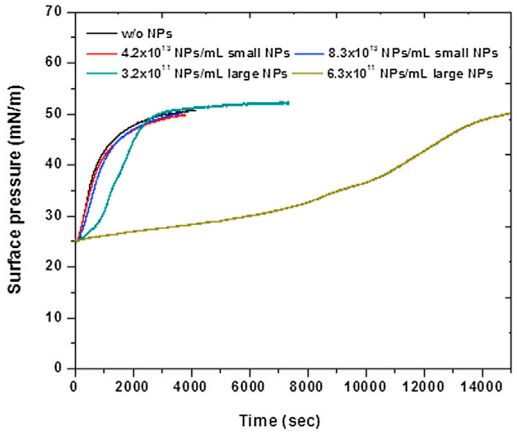

FIGURE 7 Vesicle insertion kinetic studies for DPPC/DPPG/SP-C (0.4 mol%) monolayer with different numbers of 12 nm and 136 nm NPs. The DPPC/DPPG (4:1) vesicles were inserted at 25 mN/m surface pressure. All measurements were done on 25 mM Hepes and 3 mM $CaCl_2$ as subphase at 20°C. To see this figure in color, go online.

the presence of these hydrophobic NPs. Furthermore, the NPs were confirmed to retain in the model LS film after continuous compression expansion cycles. In this study, we report that this effect of hydrophobic NPs is size dependent and that the effect of 136 nm NPs is much more structure damaging.

The surface activity of model LS films remained unaffected in the presence of 12 nm NPs, except at very high concentrations similar to the 20 nm NPs. However, with the increasing concentration of 136 nm NPs, the plateau region was considerably enhanced, rendering the surfactant film incapable of increasing the surface pressure to the desired value, thus causing potential lung surfactant dysfunction.

The AFM scans of the model LS films at the plateau region in the presence of 12 nm NPs displayed results similar to those obtained with 20 nm NPs. The 12 nm hydrophobic NPs are localized around the protrusion structures, also evidenced by the high-resolution images. The network structures consisting of multilayer protrusions are unaltered in the presence of both 12 and 20 nm hydrophobic NPs. For 136 nm NPs the lipid film was transferred at two different regions of the plateau to examine the surface topography of multilayer protrusion structures at different compressed states. The AFM scans for initial plateau regions show no significant change in the network structures. However, at the end plateau region, the network structures are laterally disrupted forming profuse multilayer protrusion structures. The 136 nm NPs can be spotted as clusters associated with the protrusion structures, also confirmed by the high-resolution images. Furthermore, we show that the profuse structures present are indeed multilayers formed due to continuous compression and not random collapse structures.

These enhanced multilayered protrusion structures can be well correlated with the enhanced plateau region in the isotherm of the model LS film in the presence of 136 nm NPs. The multilayer protrusion formation is explained by selective squeeze out of the fluid component of the film. Enhanced multilayer protrusion formation implies an increased amount of lipid molecules in the fluid component of the film. In addition, lateral disruption of the network structures implies increased mixing of rigid and fluid domains, i.e., decreased phase separation. Furthermore, the LS model film does not exhibit any variation in the hysteresis of the isotherm in the presence of any of the NPs with respect to multiple compression reexpansion cycles. Hence, the NPs are retained in the surfactant film possibly due to their highly hydrophobic surface and consequently high free energy barrier to enter into the subphase.

The isotherms for bare NPs illustrate high surface activity of the 136 nm NPs suggesting a high-energy barrier encountered by the 136 nm hydrophobic NPs for penetrating into the aqueous subphase. This phenomenon also partially explains the noncollapse behavior of the LS model system in the presence of the 136 nm NPs even after continuous compression. The hydrophobic NPs interact with the hydrophobic acyl chains of the lipid molecules and retain the lipid molecules along with it preventing collapse. We expect a similar interaction in the case of 12 nm NPs; however, it is not prominently visible in these data sets.

Because DPPC forms the major component of the model LS film, any alteration in its phase behavior due to the presence of differently sized NPs can be extrapolated to the model LS film. Hence, the size-dependent effect of NPs on phase behavior and domain morphology of DPPC monolayers was studied. The isotherm of a DPPC monolayer did not display any appreciable change in the presence of 12 nm NPs. However, in the presence of 136 nm NPs, the LE-LC coexistence region was diminished. To emphasize the effect of 136 nm NPs on the isotherms of the DPPC monolayer, we have calculated the compressibility values at the LC phase region. With increasing concentration of 136 nm NPs the compressibility values increase, which imply decreased cooperativity between lipid molecules. Hence, 136 nm NPs interfere with the lipid packing order and decrease intermolecular interactions. This can also be true for 12 nm NPs but the isotherms data alone for 12 nm NPs are not conclusive.

The epifluorescence microscopy images reveal slightly disrupted domain morphology for DPPC monolayers in the presence of 12 nm NPs. Furthermore, due to the presence of the high numbers of these fluorescent 12 nm NPs, they are clearly visible at high surface pressure. In the presence of 136 nm NPs, however, the domain morphology is tremendously disrupted causing branching of the domains at low surface pressure and formation of mesh-like network structures at high surface pressure. The disruption in the domain morphology implies probably localization of the NPs at the phase boundaries and decreased line tension suggests decreased phase separation. This is in accordance

with the AFM scans of DPPC/DPPG/SP-C mixtures where DPPC is the major component. The lateral disruption of the network structures in the AFM scans of DPPC/DPPG/SP-C mixture are rationalized because of increased mixing of rigid and fluid domains, i.e., decreased phase separation. Hence, in the presence of 136 nm NPs, line tension between different phases is reduced largely causing mixing of domains in the lipid film, which is responsible for lateral disruption of the network structures. This increase in the fluid component causes enhanced multilayer protrusion formation consequently causing potential lung surfactant dysfunction.

A 136 nm nanoparticle should occupy around 17,000 nm^2 area on the aqueous subphase, whereas the area occupied by the lipid molecule is 0.6 nm^2, which is almost 10^6 times smaller than that of the nanoparticle. Considering that the number of lipid molecules is 10^5 per nanoparticle, the total area occupied by the 136 nm NPs should be almost of the same order as the total area occupied by the lipid molecules. Given this fact, the whole isotherm of a DPPC monolayer should be shifted toward higher area per molecule values (as opposed to expansion of LE phase region alone) to account for the area occupied by the 136 nm nanoparticle. However, this is not the case even at the highest concentration of the 136 nm NPs. This suggests that the lipid molecules are displaced from the air-water interface to the surface of the nanoparticle attributable to hydrophobic interaction between the acyl chains and the hydrophobic nanoparticle surface. Thus, it renders fewer lipid molecules on the aqueous subphase leaving the total area occupied essentially the same. In addition, it should be noticed that the transition pressure is unaltered in the presence of NPs indicating that there might be a possible phase separation between the lipid bound to the nanoparticles and the free lipid molecules.

The presence of 136 nm NPs also has a significant effect on the vesicle insertion process as seen from the vesicle insertion kinetics studies. The vesicle insertion process is thought to be a two-step mechanism—initial Ca^{+2}-mediated adsorption of the vesicles onto the model LS monolayer, rupture of the vesicles, and reincorporation of the lipids from the vesicles into the monolayer facilitated by surfactant proteins. As seen in Fig. 7, the presence of higher numbers of 12 nm NPs has a negligible effect on the insertion kinetics of the model LS film. At very high concentrations, the inhibition effect of these NPs is much more prominent (data not shown) where the half-time increases with increasing concentration. These results are similar to those observed with the 20 nm diameter NPs. In the presence of 136 nm NPs the inhibitory effect is visibly prominent even at comparatively lower numbers of NPs. Another important observation is that the shape of the curve is hyperbolic in the presence of 12 nm NPs and sigmoidal in the presence of 136 nm NPs. The inhibitory effect of the 12 nm NPs can be explained by a direct or indirect interaction of the NPs with the surfactant protein-C, thus inhibiting its function in vesicle insertion. This is also emphasized by the fact that the isotherm of model LS monolayers show inhibited plateau regions in the presence of very high concentrations of 12 nm NPs. As previously discussed, these NPs are known to be found associated with the protrusion structures and hence with the fluid component of the film. The surfactant-specific proteins are also known to be present in the DPPG-enriched fluid component of the film. This increases the possibility of an interaction between the surfactant protein-C and the 12 nm nanoparticle, which is observable only at very high concentrations of the NPs. The effect of 136 nm nanoparticles on the vesicle insertion curve however is significantly different and cannot be simply explained with the previous theory of nanoparticle-protein interaction. From the previous discussion, we deduced a possible interaction of the fluid component of the model LS film with the nanoparticles. The fluid component is mainly enriched in DPPG. DPPG being negatively charged is also involved in the adsorption of the vesicles, mediated by Ca^{+2} ions, and plays an important role in the electrostatic interaction between the lipid monolayer and the LUVs in the subphase (33,34). In the presence of 136 nm NPs, DPPG molecules may possibly form a lipid layer on the nanoparticle and hence the number of DPPG molecules available for adsorption of LUVs would decrease leading to an initial lag phase in the insertion curve. With the eventual adsorption and reincorporation of the new lipid material from the subphase to the monolayer, the number of DPPG molecules in the monolayer increases subsequently leading to an increased adsorption of the vesicles. This process is similar to a cooperative process and hence would result in a sigmoidal curve as obtained in Fig. 7. Due to its size, 136 nm NPs have much more area to occupy larger amounts of lipid molecules than the 12 nm NPs. Hence, even a small number of 136 nm NPs has a considerably higher inhibitory effect on the insertion kinetics than the 12 nm NPs.

CONCLUSION

This study shows the effect of different sized NPs on model LS films and proves that the size of the NPs is an important factor responsible for causing severe structural and functional damage to the model LS films. The surface activity of the model LS film is almost unaffected in the presence of 12 nm NPs, which is similar to the results obtained for 20 nm NPs. However, in the presence of 136 nm NPs the plateau region is enhanced significantly rendering the model LS film highly compressible. The AFM scans reveal formation of profuse multilayer protrusion structures responsible for the enhanced plateau region. The fluorescence microscopy images for DPPC monolayers in the presence of 136 nm NPs show a decreased tendency for a phase separation due to reduction in the line tension. This is in

accordance with the AFM studies where the network structure of model LS film is disrupted in the presence of 136 nm NPs implying diffusive mixing of rigid and fluid domains. The vesicle insertion kinetics is inhibited in the presence of fewer numbers of 136 nm NPs as compared with the 12 nm NPs where the effect is negligible. The mechanism for the inhibitory effect is also discussed in the study based on the size of the NPs. It is worth noticing that fewer numbers of 136 nm NPs have much more structural and functional damaging effect than the comparatively higher number of 12 nm NPs.

SUPPORTING MATERIAL

Seven figures are available at http://www.biophysj.org/biophysj/supplemental/S0006-3495(13)01246-0.

We acknowledge Amit Kumar Sachan for fruitful discussions especially regarding the high pressure measurements on the film balance.

This work was supported by the Deutsche Forschungsgemeinschaft, Schwerpunktprogramm 1313 and by the NRW International Graduate School of Chemistry Münster.

REFERENCES

1. Goerke, J. 1974. Lung surfactant. *Biochim. Biophys. Acta.* 344:241–261.
2. Hills, B. A. 1990. The role of lung surfactant. *Br. J. Anaesth.* 65:13–29.
3. Schürch, S., J. Goerke, and J. A. Clements. 1976. Direct determination of surface tension in the lung. *Proc. Natl. Acad. Sci. USA.* 73:4698–4702.
4. Yu, S., P. G. R. Harding, …, F. Possmayer. 1983. Bovine pulmonary surfactant: chemical composition and physical properties. *Lipids.* 18:522–529.
5. Goerke, J. 1998. Pulmonary surfactant: functions and molecular composition. *Biochim. Biophys. Acta.* 1408:79–89.
6. Veldhuizen, R., K. Nag, …, F. Possmayer. 1998. The role of lipids in pulmonary surfactant. *Biochim. Biophys. Acta.* 1408:90–108.
7. Veldhuizen, E. J. A., and H. P. Haagsman. 2000. Role of pulmonary surfactant components in surface film formation and dynamics. *Biochim. Biophys. Acta.* 1467:255–270.
8. Weaver, T. E., and J. J. Conkright. 2001. Function of surfactant proteins B and C. *Annu. Rev. Physiol.* 63:555–578.
9. Reid, K. B. M. 1998. Functional roles of the lung surfactant proteins SP-A and SP-D in innate immunity. *Immunobiology.* 199:200–207.
10. Schürch, S., R. Qanbar, …, F. Possmayer. 1995. The surface-associated surfactant reservoir in the alveolar lining. *Biol. Neonate.* 67 (*Suppl 1*):61–76.
11. Amrein, M., A. von Nahmen, and M. Sieber. 1997. A scanning force- and fluorescence light microscopy study of the structure and function of a model pulmonary surfactant. *Eur. Biophys. J.* 26:349–357.
12. Krol, S., M. Ross, …, A. Janshoff. 2000. Formation of three-dimensional protein-lipid aggregates in monolayer films induced by surfactant protein B. *Biophys. J.* 79:904–918.
13. Pérez-Gil, J. 2008. Structure of pulmonary surfactant membranes and films: the role of proteins and lipid-protein interactions. *Biochim. Biophys. Acta.* 1778:1676–1695.
14. Rugonyi, S., S. C. Biswas, and S. B. Hall. 2008. The biophysical function of pulmonary surfactant. *Respir. Physiol. Neurobiol.* 163:244–255.
15. Oosterlaken-Dijksterhuis, M. A., H. P. Haagsman, …, R. A. Demel. 1991. Characterization of lipid insertion into monomolecular layers mediated by lung surfactant proteins SP-B and SP-C. *Biochemistry.* 30:10965–10971.
16. Ross, M., S. Krol, …, H. J. Galla. 2002. Kinetics of phospholipid insertion into monolayers containing the lung surfactant proteins SP-B or SP-C. *Eur. Biophys. J.* 31:52–61.
17. Mühlfeld, C., B. Rothen-Rutishauser, …, P. Gehr. 2008. Interactions of nanoparticles with pulmonary structures and cellular responses. *Am. J. Physiol. Lung Cell. Mol. Physiol.* 294:L817–L829.
18. Konduru, N. V., Y. Y. Tyurina, …, V. E. Kagan. 2009. Phosphatidylserine targets single-walled carbon nanotubes to professional phagocytes in vitro and in vivo. *PLoS ONE.* 4:e4398.
19. Kapralov, A. A., W. H. Feng, …, V. E. Kagan. 2012. Adsorption of surfactant lipids by single-walled carbon nanotubes in mouse lung upon pharyngeal aspiration. *ACS Nano.* 6:4147–4156.
20. Schleh, C., C. Muhlfeld, …, J. M. Hohlfeld. 2009. The effect of titanium dioxide nanoparticles on pulmonary surfactant function and ultrastructure. *Resp. Res.* 10:90.
21. Fan, Q. H., Y. E. Wang, …, Y. Y. Zuo. 2011. Adverse biophysical effects of hydroxyapatite nanoparticles on natural pulmonary surfactant. *ACS Nano.* 5:6410–6416.
22. Harishchandra, R. K., M. Saleem, and H. J. Galla. 2010. Nanoparticle interaction with model lung surfactant monolayers. *J. R. Soc. Interface.* 7 (*Suppl 1*):S15–S26.
23. Bakshi, M. S., L. Zhao, …, N. O. Petersen. 2008. Metal nanoparticle pollutants interfere with pulmonary surfactant function in vitro. *Biophys. J.* 94:855–868.
24. Nel, A., T. Xia, …, N. Li. 2006. Toxic potential of materials at the nanolevel. *Science.* 311:622–627.
25. Sachan, A. K., R. K. Harishchandra, …, H. J. Galla. 2012. High-resolution investigation of nanoparticle interaction with a model pulmonary surfactant monolayer. *ACS Nano.* 6:1677–1687.
26. Krol, S., A. Janshoff, …, H. J. Galla. 2000. Structure and function of surfactant protein B and C in lipid monolayers: a scanning force microscopy study. *Phys. Chem. Chem. Phys.* 2:4586–4593.
27. von Nahmen, A., A. Post, …, M. Sieber. 1997. The phase behavior of lipid monolayers containing pulmonary surfactant protein C studied by fluorescence light microscopy. *Eur. Biophys. J.* 26:359–369.
28. von Nahmen, A., M. Schenk, …, M. Amrein. 1997. The structure of a model pulmonary surfactant as revealed by scanning force microscopy. *Biophys. J.* 72:463–469.
29. Haagsman, H. P., S. Hawgood, …, B. J. Benson. 1987. The major lung surfactant protein, SP 28-36, is a calcium-dependent, carbohydrate-binding protein. *J. Biol. Chem.* 262:13877–13880.
30. Taneva, S. G., J. Stewart, …, K. M. W. Keough. 1998. Method of purification affects some interfacial properties of pulmonary surfactant proteins B and C and their mixtures with dipalmitoylphosphatidylcholine. *Biochim. Biophys. Acta.* 1370:138–150.
31. Scherer, C., S. Utech, …, M. Maskos. 2010. Synthesis, characterization and fine-tuning of bimodal poly(organosiloxane) nanoparticles. *Polymer (Guildf.).* 51:5432–5439.
32. Schärtl, W. 2007. Light Scattering from Polymer Solutions and Nanoparticle Dispersions. Springer, Berlin Heidelberg.
33. Jungmann, N., M. Schmidt, …, J. Ebenhoch. 2002. Synthesis of amphiphilic poly(organosiloxane) nanospheres with different core-shell architectures. *Macromolecules.* 35:6851–6857.
34. Koshkina, O., C. Bantz, …, M. Maskos. 2011. Fluorophore-labeled siloxane-based nanoparticles for biomedical applications. *Macromol. Symp.* 309–310:141–146.